Heliyon 10 (2024) e32699

Contents lists available at ScienceDirect

Heliyon

journal homepage: www.cell.com/heliyon

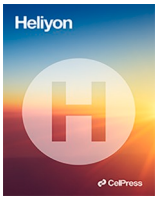

Research article

Amide proton transfer-weighted and arterial spin labeling imaging may improve differentiation between high-grade glioma recurrence and radiation-induced brain injury

Ling Chen [a,1], Lizhao Huang [a,1], Jinhuan Zhang [a], Shuanghong Li [a], Yao Li [b], Lifang Tang [a], Weijiao Chen [a], Min Wu [a], Tao Li [a,*]

[a] Department of Radiology, Liuzhou Workers Hospital, Guangxi, China
[b] Department of Neurosurgery, Liuzhou Workers Hospital, Guangxi, China

ARTICLE INFO

Keywords:
High-grade glioma
APTw
ASL
Tumor recurrence
Radiation-induced brain injury

ABSTRACT

Rationale and objectives: The management of tumor recurrence (TR) and radiation-induced brain injury (RIBI) poses significant challenges, necessitating the development of effective differentiation strategies. In this study, we investigated the potential of amide proton transfer-weighted (APTw) and arterial spin labeling (ASL) imaging for discriminating between TR and RIBI in patients with high-grade glioma (HGG).

Methods: A total of 64 HGG patients receiving standard treatment were enrolled in this study. The patients were categorized based on secondary pathology or MRI follow-up results, and the demographic characteristics of each group were presented. The APTw, rAPTw, cerebral blood flow (CBF) and rCBF values were quantified. The differences in various parameters between TR and RIBI were assessed using the independent-samples *t*-test. The discriminative performance of these MRI parameters in distinguishing between the two conditions was assessed using receiver operating characteristic (ROC) curve analysis. Additionally, the Delong test was employed to further evaluate their discriminatory ability.

Results: The APTw and CBF values of TR were significantly higher compared to RIBI ($P < 0.05$). APTw MRI demonstrated superior diagnostic efficiency in distinguishing TR from RIBI (area under the curve [AUC]: 0.864; sensitivity: 75.0 %; specificity: 81.8 %) when compared to ASL imaging. The combined utilization of APTw and CBF value further enhanced the AUC to 0.922. The Delong test demonstrated that the combination of APTw and ASL exhibited superior performance in the identification of TR and RIBI, compared to ASL alone ($P = 0.048$).

Conclusion: APTw exhibited superior diagnostic efficacy compared to ASL in the evaluation of TR and RIBI. Furthermore, the combination of APTw and ASL exhibits greater discriminatory capability and diagnostic performance.

Abbreviations: APTw Amide proton transfer-weighted, **ASL** arterial spin labeling; **HGG** high-grade glioma, **TR** tumor recurrence; **RIBI** radiation-induced brain injury, **CBF** cerebral blood flow; **ROC** receiver operating characteristic, **AUC** area under the curve; **TMZ** temozolomide chemotherapy, **MRS** Magnetic Resonance Spectroscopy; **Cho** choline, **Cr** creatine.

* Corresponding author.
E-mail address: li966511@163.com (T. Li).

[1] First authorship: Ling Chen and Lizhao Huang contributed equally to this work and share first authorship.

https://doi.org/10.1016/j.heliyon.2024.e32699
Received 8 February 2024; Received in revised form 5 June 2024; Accepted 6 June 2024
Available online 7 June 2024

1. Introduction

High-grade gliomas (HGG), as prevalent primary brain tumors in adults, are characterized by their infiltrative nature and inherent resistance to treatment, resulting in a dismal prognosis [1–3]. The standard treatment for HGG following surgical intervention entails the integration of radiotherapy and temozolomide chemotherapy (TMZ), in conjunction with six cycles of adjuvant TMZ chemotherapy administration [4]. Despite aggressive therapeutic interventions, TR and RIBI remain prevalent issues in various medical conditions due to their distinct treatment strategies [5,6]. This persistent challenge often frustrates healthcare professionals and patients alike, as it hampers the effectiveness of standard treatment protocols. TR often requires additional interventions such as surgery, chemotherapy, or targeted therapies to control tumor cell growth [7]. Conversely, RIBI focuses on symptom control and supportive care since there is currently no specific treatment available to reverse the pathological changes caused by radiation. Therefore, the identification of a robust approach to differentiate between TR and RIBI in the postoperative management of HGG has emerged as an imperative issue that necessitates immediate resolution.

Currently, histopathological diagnosis obtained through biopsy or surgical resection remains the gold standard for diagnosing TR or RIBI in accordance with established medical practices. However, invasive procedures carry inherent risks and may not always be feasible, especially when dealing with lesions located in critical areas of the brain [8]. Additionally, histopathological analysis may not always yield definitive results due to the challenge of distinguishing between tumor cells and radiation therapy-induced changes in cases involving extensive radiation therapy [9]. The Response Assessment in Neuro-Oncology (RANO) guidelines recommend utilizing MRI for evaluating tumor response post-therapy [10,11]. However, both TR and RIBI exhibit comparable imaging characteristics on conventional MRI, posing challenges in distinguishing between these two conditions due to their shared features of irregular enhancement at surgical margins and significant peritumoral edema.

Considering that angiogenesis and high proliferation activity are reliable diagnostic indicators of HGG recurrence [12], APTw and ASL imaging techniques incorporating these pathological features show promise in distinguishing TR from RIBI. APTw imaging measures the concentration of endogenous mobile proteins, reflecting tumor cell metabolism [13,14]. The increased intensity of the APTw signal indicates an upregulation in protein metabolism and potentially signifies tumor recurrence [15]. The association between APTw values and the tissue proliferation index of Ki-67 has been consistently demonstrated in several studies, highlighting a close correlation between protein metabolism and tumor aggressiveness [16–18]. Additionally, mounting evidence indicates that APTw imaging plays a crucial role in tumor grading and monitoring treatment response. ASL, on the other hand, is a non-invasive MRI perfusion imaging that enables assessment of capillary microcirculation within the lesion by quantifying blood flow [19–21]. Several studies have evaluated the efficacy of PWI in differentiating radiation necrosis from tumor progression [22,23]. Recurrent brain tumors exhibited significantly elevated levels of vascular expression in comparison to RIBI, as observed through histological analyses.

In this study, we hypothesized that the combination of APTw and ASL techniques could provide a more comprehensive assessment of tumor biology in comparison to conventional MRI. Therefore, our objective was to investigate the potential of APTw and ASL imaging for discriminating between TR and RIBI among patients with HGG.

2. Materials and methods

2.1. Subjects

This study was approved by the ethics committee of Liuzhou Workers Hospital. All individual participants signed the consent form prior to the MR study. This study was conducted from October 2020 to December 2023. A total of 76 patients (14 males, aged 56.5 ± 14.0 years) receiving standard treatment were enrolled in this study. The primary diagnosis of HGG included anaplastic astrocytoma (n = 31), anaplastic oligodendroglioma (n = 7), and glioblastoma (n = 38). Patients were selected based on the following criteria [1]: histological examination confirming the presence of HGG [2]; administration of radiotherapy or chemoradiotherapy after surgical resection [3]; observation of new or expanded enhancement lesions after treatment through APTw, ASL and Gd-enhanced T1w imaging examinations. Severe motion artifacts or tumors with alternative histopathologic diagnoses were excluded from the study. Final diagnosis for all patients was confirmed by a second surgical resection or subsequent MRI examinations. Regular MRI follow-up assessments were conducted every 2–3 months, with a minimum follow-up period of 6 months.

2.2. MRI protocols

MRI examinations were performed using a 3.0 T MRI system (Ingenia CX, Philips Medical Systems, Best, The Netherlands). A 32-channel head coil was used to perform the MRI scans. The conventional MRI sequences consisted of T1WI (TR = 2000 ms, TE = 19 ms, FOV = 24 × 24 cm, section thickness = 4 mm, NEX = 1, matrix = 256 × 256), T2WI (TR = 4000 ms, TE = 122 ms, FOV = 240 × 240 mm2, section thickness = 4 mm, NEX = 1, matrix = 256 × 256), and T2 fluid-attenuated inversion recovery (FLAIR) imaging (TR = 10,000 ms, TE = 125 ms, FOV = 240 × 240 mm2, section thickness = 4 mm, NEX = 1, matrix = 256 × 256) sequences. Prior to contrast material administration, advanced imaging techniques including three-dimensional pCASL, and APTw imaging were performed. The whole brain 3D pCASL sequence was performed prior to the administration of contrast medium, with the following parameters: post-labeling delay delay = 1.5s, TR = 4.4 s, TE = 9.2 ms, acquisition matrix = 8 arms with 512 spiraling points, NEX = 3, section thickness = 32 mm, FOV = 240 × 240 mm, bandwidth = 62.5, plane axial orientation. The ASL mapping was created by subtracting the unlabeled image from the labeled image. 3D APTw imaging was carried out using a multiple source transmitting technology, which has the potential to both extend the radio frequency saturation time and boost APT efficiency. 3D mDIXON TSE sequence was used. The

acquisition parameters were: TR = 1980 ms, TE = 19 ms, FOV = 240 × 240 mm, section thickness = 4 mm, NEX = 1, matrix = 256 × 256, voxel size = 1.65 × 3.15 × 6.00 mm^3. Following intravenous administration of Gadoterate meglumine at a dose of 0.2 mL/kg body weight with a flow rate of 2 mL/s via the median cubital vein, post-contrast T1-weighted images were acquired.

2.3. Image analysis

3D APTw and pCASL data were analyzed on the workstation using a commercially-available software (Ingenia, Philips Medical Systems, CX, Intellispace Portal 10.1). The ASL and APTw images were resampled through linear interpolation to match the resolution of Gd images, followed by rigid registration through a custom MatLab program for coregistration. In this study, the confirmation of TR or RIBI is based on the standard response assessment of RANO glioma or re-operative pathologic diagnosis. Regions of interest (ROIs) were carefully selected in a double-blind manner by two experienced neuroradiologists, each with fifteen and twelve years of expertise. An interclass correlation coefficient value between 0.75 and 1 indicated good agreement. Any disagreement between the two neuroradiologists was resolved by consensus. Six ROIs with an area of 0.50 cm^2 were placed in the enhanced area (EA), the peritumoral T2WI hyperintense area (PHA) and the contralateral normal white matter (CNAWM). Additionally, the same number and size of ROIs were overlaid on CBF and APTw imaging to calculated their average values. Each ROI had a standardized size of 20 pixels. To ensure accuracy, any cystic, necrotic, or bleeding parts of the lesion were excluded from analysis. The APTw and CBF values for each ROI were recorded for every patient, followed by calculation of their respective mean APTw and CBF values. Furthermore, to minimize potential errors in measurement, we also documented relative APTw (rAPTw = APTw/APTwCNAWM). The calculation for relative CBF (rCBF) was the same.

2.4. Statistical analysis

The statistical analyses were performed using SPSS 27.0 software. All described results are reported as medians with ranges or 95 % confidence intervals (CIs) for continuous variables and as frequencies or percentages for categorical variables. Prior to analysis, all imaging parameters were assessed for normality using the D'Agostino-Pearson test. All parameters were normally distributed. The differences in various parameters between TR and RIBI were assessed using the independent-samples *t*-test. The discriminative performance of these MRI parameters in distinguishing between the two conditions was assessed using receiver operating characteristic (ROC) curve analysis. Additionally, the Delong test was employed to further evaluate their discriminatory ability. The correlation analysis of CBF, rCBF, APTw and rAPTw was also conducted. P value < 0.05 was considered statistically significant.

3. Results

3.1. Patient data, pathological and MRI follow-up results

The demographic characteristics of the 64 patients are summarized in Table 1. Twenty-nine patients were diagnosed with TR (12 males, 54.9 ± 12.5; 17 females, aged 52.4 ± 17.3), while the remaining 35 were diagnosed with RIBI (18 males, aged 49.6 ± 10.5; 17 females, aged 50.2 ± 11.3). Among them, there were 25 pathologically confirmed cases (23 TR and 2 RIBI) and 39 cases that were confirmed based on follow-up examinations (6 TR and 33 RIBI). During a 6-month MRI follow-up period, 33 cases were classified as RIBI. The Gd-T1WI sequences demonstrated the size of enhanced lesions decreased or disappeared completely after RIBI follow-up. In contrast, among the 29 cases diagnosed as TR, there was a significant increase in the size of the enhanced lesions and invasion into the corpus callosum and lateral ventricles.

Among the TR cases, it is noteworthy that there were 16 cases of local recurrence, 11 cases of distant recurrence, and 2 cases of subarachnoid metastasis. On Gd-T1WI, the lesions exhibited invasion into various brain regions including the lateral ventricles (n = 21), corpus callosum (n = 13), basal ganglia (n = 9), brainstem (n = 3), and cerebellum (n = 4). The surgical margin lesions displayed nodular and lump-like enhancement. In cases involving RIBI, enhanced T1-weighted images predominantly revealed the presence of lesions within the white matter region encompassing the radiotherapy field or in close proximity to the surgical remnant, exhibiting a characteristic geographic enhancement pattern. Furthermore, varying degrees of edema were observed surrounding both TR and RIBI lesions.

Table 1
Clinical information.

Variable	TR (N = 29)	RIBI(N = 35)	*P*
Age	54.9 ± 12.5	49.6 ± 10.5	0.073
No. of male patients	12 (41.4 %)	18 (51.4 %)	0.247
No. of patients who underwent a second surgery	23 (79.3 %)	2 (5.7 %)	<0.001
KPS	74.62 ± 9.17	89.48 ± 11.58	<0.001

TR: tumor recurrence; RIBI: radiation-induced brain injury; KPS: karnofsky Performance Status.

3.2. Results for the enhanced and peritumoral regions

Fig. 1 depicts MR images of a representative patient diagnosed with TR, demonstrating a lesion in the left temporal lobe exhibiting significantly heterogeneous enhancement. Importantly, this enhancing lesion is characterized by remarkably high and red signal intensities on both CBF and APTw maps.

Fig. 2 illustrates MR images of a representative patient diagnosed with RIBI, revealing a heterogeneous Gd-enhancing lesion in the left frontal lobe. The lesions exhibited predominantly green isoperfusion on the CBF maps and scattered flaky yellow signals slightly higher than background on the APTw maps.

The results of CBF, rCBF, APTw and rAPTw values in EA and PHA between patients with TR and RIBI are presented in Table 2 and Fig. 3. The TR group exhibited significantly higher values of CBF (32.83 ± 6.18 mL/100 g/min vs. 25.06 ± 5.03 mL/100 g/min), rCBF (2.37 ± 0.86 vs. 1.44 ± 0.45), APTw (3.13 ± 0.26 % vs. 2.20 ± 0.71 %), and rAPTw (1.43 ± 0.46 vs. 1.13 ± 0.37) in the enhanced region compared to the RIBI group. Similarly, the lesions in the TR group showed significantly elevated APTw (2.38 ± 0.63 % vs. 2.02 ± 0.49 %) and rAPTw (1.26 ± 0.36 vs. 1.02 ± 0.36) values in the peritumoral area, while no significant differences were observed in CBF and rCBF between the two groups ($P = 0.983$, 0.294, respectively).

The diagnostic efficacy of ASL and APTw imaging in the enhanced and peritumoral regions is compared between the TR and RIBI groups, as depicted in Fig. 4. The ROC curve demonstrated that the APTw value exhibited the highest AUC of 0.864 (95 % CI: 0.771, 0.956) in the enhanced region for discriminating between TR and RIBI, followed by rAPTw, CBF, and rCBF values. When combined ASL and APTw imaging, the AUC increase to 0.922. However, in the peritumoral area, CBF and rCBF showed limited sensitivity and specificity in distinguishing between the two groups with AUCs not exceeding 0.60. On the other hand, APTw had an AUC of 0.672 with a sensitivity of 65.5 % and specificity of 65.7 %, while rAPTw had an AUC of 0.699 with a sensitivity of 71.4 % and specificity of 62.8 % (Table 3). Furthermore, Delong test demonstrated that the combined utilization of APTw and ASL imaging demonstrated a significant enhancement in the diagnostic accuracy of TR and RIBI when compared to ASL alone ($P = 0.048$). However, this combined approach did not exhibit a statistically significant difference in comparison to APTw imaging ($P = 0.057$).

The CBF and rCBF exhibited a significant positive correlation with APTw and rAPTw (R = 0.49, R = 0.27, R = 0.37 and R = 0.45) in the enhanced area, respectively (Fig. 5). However, no linear relationship was observed between the parameters in the peritumoral region.

4. Discussion

Advanced MRI imaging markers, particularly those indicative of tumor angiogenesis and protein metabolism, hold promise in evaluating treatment response among postoperative patients with HGG. In this study, we investigated the value of 3D pCASL and APTw techniques in differentiating between TR and RIBI among a cohort of HGG patients who underwent standard therapeutic interventions. The findings revealed that APTw exhibited superior diagnostic efficacy compared to ASL in the evaluation of postoperative recurrence and radiation-induced damage. Moreover, the combined utilization of APTw and ASL imaging improved diagnostic accuracy in distinguishing TR from RIBI when compared to using ASL alone. Importantly, it has been observed that lesions located in the PHA may also exhibit a degree of heterogeneity in comparison to those found within EA, indicating significant variations in tumor microenvironments within these regions.

The observation of morphological characteristics resembling Swiss cheese or soap bubble enhancement, as previously reported in several studies, indicates treatment-related effects [24–26]. Nevertheless, a substantial increase in lesion volume exceeding 25 %, especially when affecting vital cerebral structures like the ependyma or corpus callosum, provides strong evidence for tumor

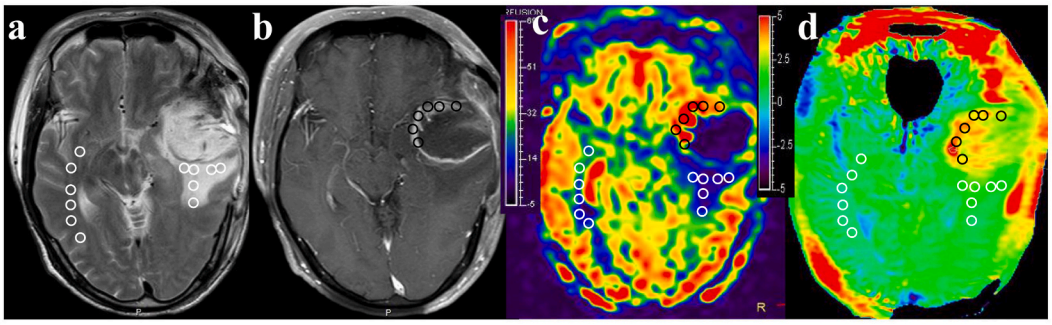

Fig. 1. The findings were observed in a 58-year-old patient with typical TR. The multiparametric MR images, including T2WI (a), Gd-enhanced T1WI (b), CBF (c), and APTw (d) maps, demonstrate a lesion in the left temporal lobe with significantly heterogeneous enhancement. Importantly, this enhancing lesion is characterized by remarkably high and red signal intensities on both CBF and APTw maps. The EA, PHA, and CNWMA were divided into six equal-sized ROIs. These ROIs were then overlaid onto the CBF and APTw maps to calculate the mean CBF and APTw values for each region. The average CBF values in TR lesion of the left temporal lobe were as follows: 58.64 mL/100 g/min for EA, 27.93 mL/100 g/min for PHA, and 24.75 mL/100 g/min for CNWMA. The average APTw values in TR lesion were as follows: 4.08 % for EA, 2.63 % for PHA, and 1.64 % for CNWMA.

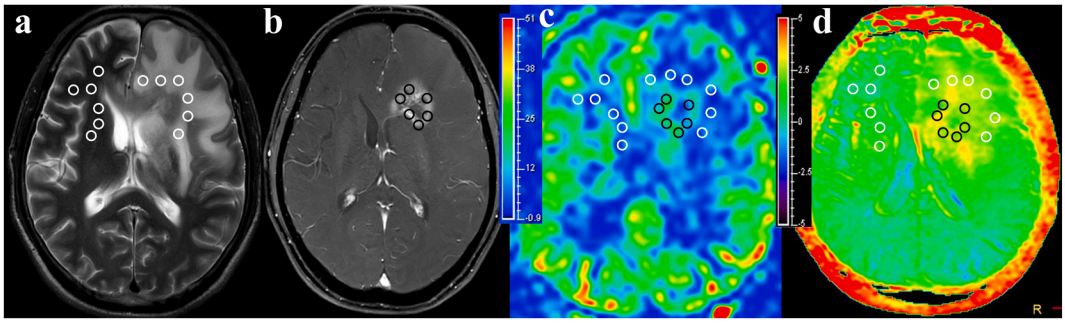

Fig. 2. The findings were observed in a 57-year-old patient with typical RIBI. Multi-parameter MR images, including T2WI (a), Gd-enhanced T1WI (b), CBF (c), and APTw (d), revealed heterogeneous enhanced lesions in the left frontal lobe. The lesions exhibited predominantly green isoperfusion on the CBF maps and scattered flaky yellow signals slightly higher than background on the APTw maps. The EA, PHA, and CNWMA were divided into six equal-sized ROIs. These ROIs were then overlaid onto the CBF and APTw maps to calculate the mean CBF and APTw values for each region. The average CBF values in RIBI lesion were as follows: 32.06 mL/100 g/min for EA, 16.28 mL/100 g/min for PHA, and 15.47 mL/100 g/min for CNWMA. The average APTw values in RIBI lesion were as follows: 2.83 % for EA, 2.23 % for PHA, and 1.81 % for CNWMA.

Table 2
Comparision of ASL and APTw parameters in EA and PHA between TR and RIBI.

Region	Variable	TR (N = 29)	RIBI(N = 35)	Diff (95 % CI)	*t*	*P*
EA	CBF (mL/100 g/min)	32.83 ± 6.18	25.06 ± 5.03	7.77 (4.97, 10.57)	5.543	<0.001
	rCBF	2.37 ± 0.86	1.44 ± 0.45	0.93 (0.59, 1.26)	5.547	<0.001
	APTw (%)	3.13 ± 0.26	2.20 ± 0.71	0.83 (0.57, 1.10)	6.201	<0.001
	rAPTw	1.43 ± 0.46	1.13 ± 0.37	0.31 (0.10, 0.52)	2.970	0.004
PHA	CBF (mL/100 g/min)	26.14 ± 4.18	26.17 ± 7.77	−0.03 (-3.25, 3.18)	0.021	0.983
	rCBF	1.19 ± 0.51	1.32 ± 0.49	−0.13 (-0.38, 0.12)	1.059	0.294
	APTw (%)	2.38 ± 0.63	2.02 ± 0.49	0.36 (0.08, 0.64)	2.536	0.014
	rAPTw	1.26 ± 0.36	1.02 ± 0.36	0.24 (0.06, 0.42)	2.671	0.010

TR: tumor recurrence; RIBI: radiation-induced brain injury; CI: confidence interval; CI: confidence interval.

recurrence [27,28]. The determination can be made by comparing consecutive MRI scans during follow-up or histopathology obtained from subsequent surgical procedures. In this study, RIBI lesions demonstrated a reduction in size or complete disappearance of enhanced lesions during the follow-up period. Conversely, the enhanced lesions observed in 29 cases diagnosed as TR demonstrated a significant increase in volume, particularly infiltrating various structures such as the corpus callosum and lateral ventricles, which is consistent with previous findings. Although routine MRI provides evidence of morphological changes to distinguish between the two, its validity may be compromised by the challenges associated with subjective image interpretation. Furthermore, prolonged follow-up periods occasionally result in missed treatment opportunities for patients.

The application of APTw or ASL imaging has been employed to differentiate between TR and RIBI in glioma patients, exhibiting promising potential. Recent studies have produced comparable preliminary findings. One study encompassed 30 cases of gliomas, and the results revealed that both ASL and APTw imaging hold promise in differentiating between treatment response and TR, the AUCs were 0.90 and 0.87 for rCBF and APTw, respectively [29]. In another study involving 43 patients with post-treatment gliomas who underwent both APTw and MET-PET imaging, the results demonstrated that APTw exhibited superior diagnostic performance, as indicated by an AUC of 0.88 [30]. Furthermore, Park et al. demonstrated that the utilization of APTw imaging as an imaging biomarker could potentially enhance the discriminative capability between recurrent gliomas and treatment-induced changes [31]. Zhang et al. found that integration of diffusion and perfusion MRI techniques enhanced the predictive capability of the radiomics model for glioma patients [32]. Another recent study confirmed significantly higher CBF values in glioma recurrence patients compared to those with pseudo-progression [33]. Our findings further support these results and indicate that the APTw and ASL could be used as effective imaging biomarkers to identify TR and RIBI in HGG patients. Importantly, APTw demonstrated superior diagnostic accuracy compared to ASL imaging in discriminating TR from RIBI, with AUC values of 0.838 and 0.864 for ASL and APTw.

Furthermore, our results revealed that the integration of APTw and ASL imaging techniques has been found to significantly enhance the accuracy of diagnostic assessments. Combining these two modalities enables earlier detection and characterization of subtle changes in tissue composition or blood flow dynamics. Therefore, the integration of these two techniques enables a more precise assessment of tumor microenvironment, thereby enhancing the differentiation between TR and RIBI. From a pathogenic point of view, the greater APTw signal intensity in TR could be due to heightened levels of mobile proteins and peptides, which are associated with increased cellularity and cellular proliferation [34,35]. The altered perfusion patterns on ASL in TR are caused by angiogenesis-related aberrant blood flow patterns and increased microvascular density [33]. Conversely, in radiation damage, tissue necrosis and vascular damage brought on by radiation therapy result in a reduction in cellular metabolism and perfusion [36,37]. APTw and CBF levels that are both elevated suggest that glioma recurrence may be possible. On the other hand, radiation damage is present when both the CBF

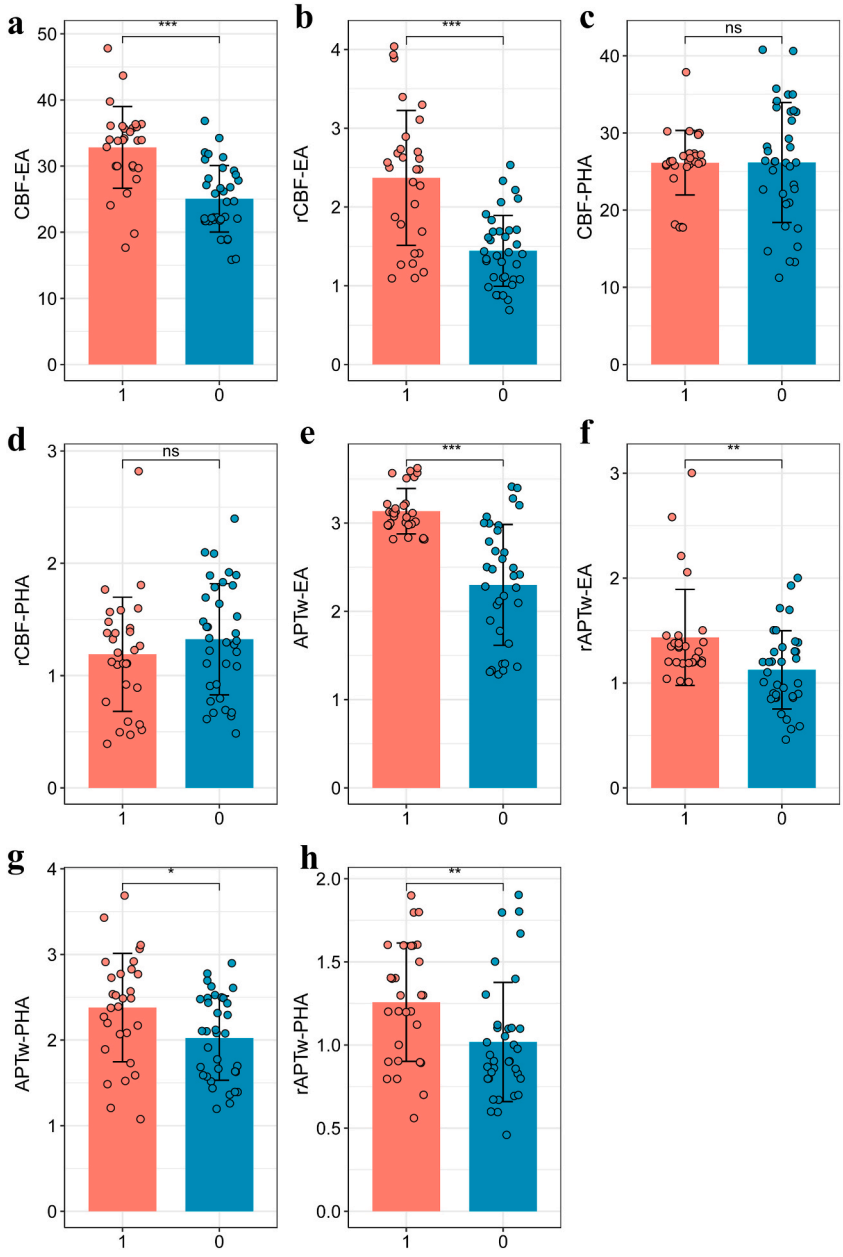

Fig. 3. Comparisons of parameters in the EA and PHA between TR and RIBI.
EA: enhanced area; PHA: peritumoral T2WI hyperintense area; TR: tumor recurrence; RIBI: radiation-induced brain injury.

and APTw levels fall at the same time. This information is essential for choosing the right course of treatment since radiation necrosis can be treated conservatively or with anti-inflammatory drugs, whereas glioma recurrence may require more surgery or chemotherapy.

The value of differentiating the tumor core from the peritumoral edema region has been investigated [38–41]. Within the enhanced region, significantly higher CBF and APTw values were observed in the TR groups compared to the RIBI groups that the peritumoral edema of RIBI may be related to vasogenic edema, while the peritumoral edema of glioma may be related to the invasion of tumor cells, thus confirming previous findings. Importantly, a significant positive correlation between CBF and APTw ($R = 0.49$, $P < 0.001$) was found in the enhanced area ($R = 0.49$, $P < 0.001$). Furthermore, notable differences in APTw values between these groups were also observed within the peritumoral edema region, while there was no statistically significant difference in CBF values. This suggests that APTw imaging may exhibit greater sensitivity to changes in the tumor microenvironment compared to ASL imaging. One potential explanation for the notable disparity in APTw values may stem from the earlier and more pronounced cellular proliferation relative to angiogenesis, or the heightened sensitivity of APTw imaging compared to ASL imaging in capturing alterations within the tumor

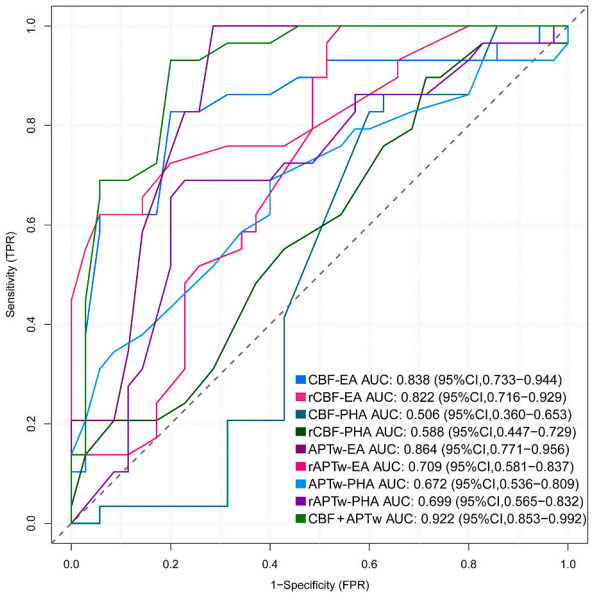

Fig. 4. The ROC curve for discriminating between TR and RIBI based on APTw and ASL imaging in the EA and PHA.
EA: enhanced area; PHA: peritumoral T2WI hyperintense area; TR: tumor recurrence; RIBI: radiation-induced brain injury; CI: confidence interval.

Table 3
ROC analysis results were obtained based on APTw, rAPTw, CBF, and rCBF values in the EA and PHA of TR and RIBI.

Region	Parameter	AUC	Cut-off	95 % CI	Sensitivity	Specificity	*P*
EA	CBF	0.838	29.5	0.733–0.943	0.828	0.8	<0.001
	rCBF	0.822	1.75	0.716–0.928	0.724	0.8	<0.001
	APTw	0.864	2.75	0.771–0.956	1	0.714	<0.001
	rAPTw	0.709	2.15	0.580–0.855	0.828	0.629	0.003
PHA	CBF	0.506	19.5	0.360–0.653	0.628	0.415	0.930
	rCBF	0.588	1.15	0.272–0.552	0.517	0.673	0.230
	APTw	0.672	2.35	0.591–0.864	0.655	0.657	0.003
	rAPTw	0.699	1.55	0.149–0.401	0.714	0.628	0.002

EA: enhanced area; PHA: peritumoral T2WI hyperintense area; TR: tumor recurrence; RIBI: radiation-induced brain injury; CI: confidence interval.

microenvironment. The rapid proliferation of glioma cells is well-established, leading to an increased cell density within the peritumoral edema region [42]. The increased cell density suggests higher levels of movable proteins and peptides, which may lead to more prominent APTw signaling.

There are several limitations in our study that warrant acknowledgment. Firstly, the small sample size may restrict the generalizability of our findings. A larger sample size would yield more robust results and facilitate subgroup analysis to explore potential confounding factors. Additionally, the irregular morphology of TR and RIBI presents challenges for quantitative analysis of the entire tumor, thereby restricting us to obtaining only an average value from the largest plane. This approach may introduce bias and compromise result accuracy. In future studies, investigating alternative methods such as histogram analysis or radiomics-based approaches will contribute to a deeper understanding of the tumor microenvironment.

In conclusion, APTw imaging may exhibit superiority over ASL imaging in distinguishing between TR and RIBI among patients with HGG. The integration of ASL and APTw techniques has significantly enhanced our ability to accurately diagnose these conditions, providing valuable insights into tumor recurrence and treatment response.

Ethical Approval

All procedures conducted in studies involving human participants adhered to the ethical standards set by the ethics committee of Liuzhou Workers Hospital (Approval number: KY2021085).

Informed consent

Informed consent was obtained from all individual partici-pants included in the study and consented to have these images published.

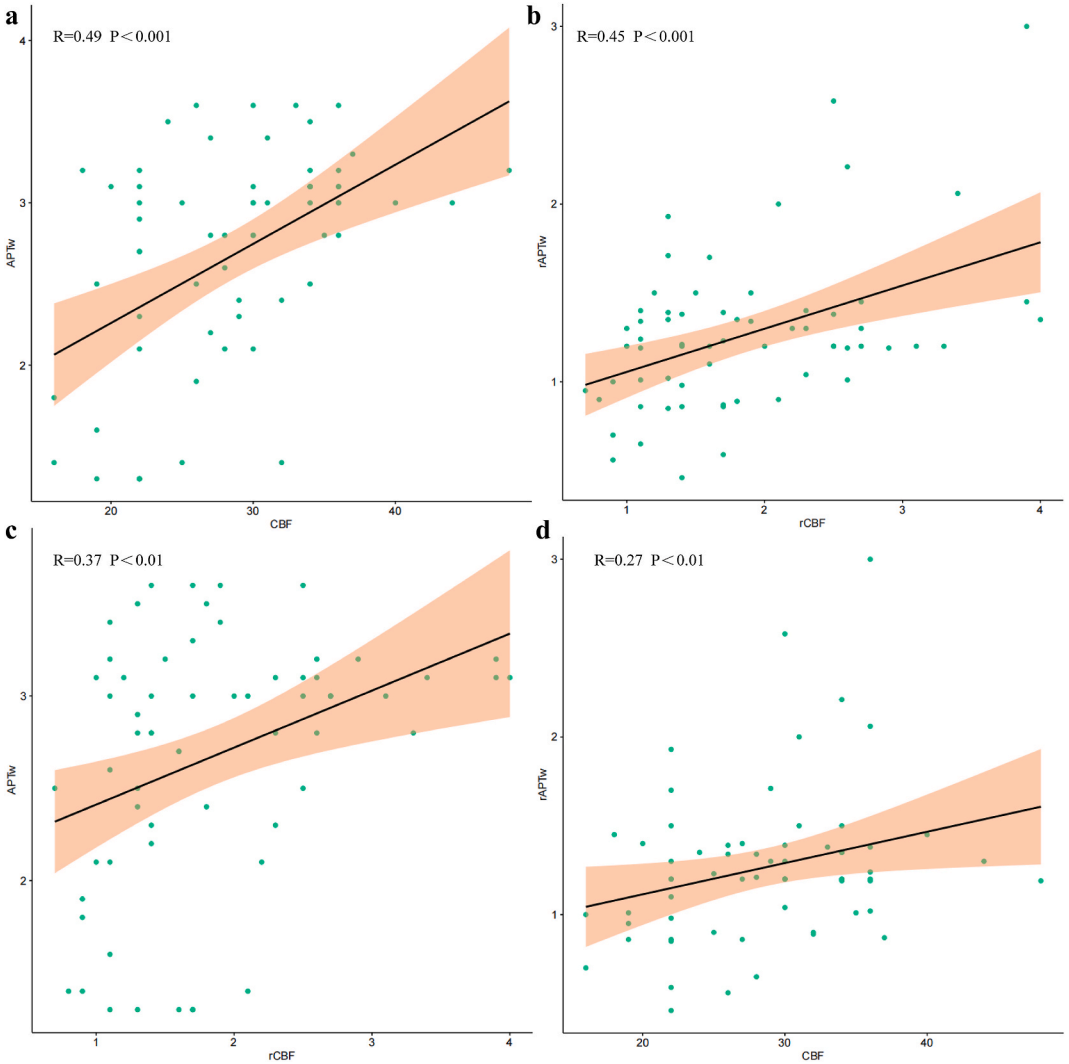

Fig. 5. The relationship between CBF and APTw in the enhanced area was investigated. The CBF and rCBF demonstrated a significant positive correlation with APTw and rAPTw (R = 0.49, R = 0.27, R = 0.37 and R = 0.45), respectively. *** means $P < 0.001$,** means $P < 0.01$,* means $P < 0.05$.

Data availability statement

The raw data supporting the conclusions of this article will be made available by the authors, without undue reservation.

CRediT authorship contribution statement

Ling Chen: Writing – review & editing, Writing – original draft, Conceptualization. **Lizhao Huang:** Visualization, Software. **Jinhuan Zhang:** Software, Project administration. **Shuanghong Li:** Visualization, Validation. **Yao Li:** Supervision, Software. **Lifang Tang:** Methodology, Data curation. **Weijiao Chen:** Formal analysis, Data curation. **Min Wu:** Project administration, Data curation. **Tao Li:** Visualization, Validation, Supervision, Resources.

Declaration of competing interest

The authors declare that they have no known competing financial interests or personal relationships that could have appeared to influence the work reported in this paper.

Acknowledgements

This study was partially supported by grants from Guangxi Zhuang Autonomous Region self-funded project (Z20210919).

References

[1] Y. Li, Y. Liu, Y. Liang, et al., Radiomics can differentiate high-grade glioma from brain metastasis: a systematic review and meta-analysis, Eur. Radiol. 32 (11) (2022) 8039–8051.
[2] L.S. Hu, A. Hawkins-Daarud, L. Wang, et al., Imaging of intratumoral heterogeneity in high-grade glioma, Cancer Lett. 477 (2020) 97–106.
[3] Q. Zhou, C. Xue, X. Ke, et al., Treatment response and prognosis evaluation in high-grade glioma: an imaging review based on MRI, J. Magn. Reson. Imag. 56 (2) (2022) 325–340.
[4] R. Chai, S. Fang, B. Pang, et al., Molecular pathology and clinical implications of diffuse glioma, Chin Med J (Engl) 135 (24) (2022) 2914–2925.
[5] C. Li, Y. Gan, H. Chen, et al., Advanced multimodal imaging in differentiating glioma recurrence from post-radiotherapy changes, Int. Rev. Neurobiol. 151 (2020) 281–297.
[6] Y. Ozsunar, M.E. Mullins, K. Kwong, et al., Glioma recurrence versus radiation necrosis? A pilot comparison of arterial spin-labeled, dynamic susceptibility contrast enhanced MRI, and FDG-PET imaging, Acad. Radiol. 17 (3) (2010) 282–290.
[7] N. Zakhari, M.S. Taccone, C.H. Torres, et al., Prospective comparative diagnostic accuracy evaluation of dynamic contrast-enhanced (DCE) vs. dynamic susceptibility contrast (DSC) MR perfusion in differentiating tumor recurrence from radiation necrosis in treated high-grade gliomas, J. Magn. Reson. Imag. 50 (2) (2019) 573–582.
[8] J.D. Costabile, J.A. Thompson, E. Alaswad, et al., Biopsy confirmed glioma recurrence predicted by multi-modal neuroimaging metrics, J. Clin. Med. 8 (9) (2019).
[9] F. Corr, D. Grimm, B. Sass, et al., Radiogenomic predictors of recurrence in glioblastoma-A systematic review, J. Personalized Med. 12 (3) (2022).
[10] P.Y. Wen, M. van den Bent, G. Youssef, et al., Rano 2.0: update to the response assessment in neuro-oncology criteria for high- and low-grade gliomas in adults, J. Clin. Oncol. 41 (33) (2023) 5187–5199.
[11] G. Youssef, P.Y. Wen, Updated response assessment in neuro-oncology (RANO) for gliomas, Curr. Neurol. Neurosci. Rep. (2024).
[12] A. Siu, J.J. Wind, J.B. Iorgulescu, et al., Radiation necrosis following treatment of high grade glioma–a review of the literature and current understanding, Acta Neurochir. 154 (2) (2012) 191–201. ; discussion 201.
[13] I. Wamelink, J.P.A. Kuijer, B.E. Padrela, et al., Reproducibility of 3 T APT-CEST in healthy volunteers and patients with brain glioma, J. Magn. Reson. Imag. 57 (1) (2023) 206–215.
[14] J. Zhou, H.Y. Heo, L. Knutsson, et al., APT-weighted MRI: techniques, current neuro applications, and challenging issues, J. Magn. Reson. Imag. 50 (2) (2019) 347–364.
[15] K. Chen, X.W. Jiang, L.J. Deng, et al., Differentiation between glioma recurrence and treatment effects using amide proton transfer imaging: a mini-Bayesian bivariate meta-analysis, Front. Oncol. 12 (2022) 852076.
[16] S. Jiang, C.G. Eberhart, Y. Zhang, et al., Amide proton transfer-weighted magnetic resonance image-guided stereotactic biopsy in patients with newly diagnosed gliomas, Eur. J. Cancer 83 (2017) 9–18.
[17] J. Trouillas, M.L. Jaffrain-Rea, A. Vasiljevic, et al., Are aggressive pituitary tumors and carcinomas two sides of the same coin? Pathologists reply to clinician's questions, Rev. Endocr. Metab. Disord. 21 (2) (2020) 243–251.
[18] L. Zhuang, C. Lian, Z. Wang, et al., Breast-lesion assessment using amide proton transfer-weighted imaging and dynamic contrast-enhanced MR imaging, Radiol. Oncol. 57 (4) (2023) 446–454.
[19] A. Falk Delgado, F. De Luca, D. van Westen, et al., Arterial spin labeling MR imaging for differentiation between high- and low-grade glioma-a meta-analysis, Neuro Oncol. 20 (11) (2018) 1450–1461.
[20] R.E. Yoo, T.J. Yun, I. Hwang, et al., Arterial spin labeling perfusion-weighted imaging aids in prediction of molecular biomarkers and survival in glioblastomas, Eur. Radiol. 30 (2) (2020) 1202–1211.
[21] J. Lee, D.W. Park, Y.S. Kim, et al., Arterial spin labeling signal ratio between the lesion and contralateral sides for evaluation of acute middle cerebral artery infarct, Medicine 101 (2) (2022).
[22] A. Pellerin, M. Khalifé, M. Sanson, et al., Simultaneously acquired PET and ASL imaging biomarkers may be helpful in differentiating progression from pseudo-progression in treated gliomas, Eur. Radiol. 31 (10) (2021) 7395–7405.
[23] N. Pyatigorskaya, B. Sgard, M. Bertaux, et al., Can FDG-PET/MR help to overcome limitations of sequential MRI and PET-FDG for differential diagnosis between recurrence/progression and radionecrosis of high-grade gliomas? J. Neuroradiol. 48 (3) (2021) 189–194.
[24] A.J. Kumar, N.E. Leeds, G.N. Fuller, et al., Malignant gliomas: MR imaging spectrum of radiation therapy- and chemotherapy-induced necrosis of the brain after treatment, Radiology 217 (2) (2000) 377–384.
[25] C.M. Flies, K.H. van Leuken, M. Ten Voorde, et al., Conventional MRI criteria to differentiate progressive disease from treatment-induced effects in high-grade (WHO grade 3-4) gliomas, Neurology 99 (1) (2022) e77–e88.
[26] L.R. Rogers, J. Gutierrez, L. Scarpace, et al., Morphologic magnetic resonance imaging features of therapy-induced cerebral necrosis, J. Neuro Oncol. 101 (1) (2011) 25–32.
[27] D.R. Macdonald, T.L. Cascino, S.C. Schold Jr., et al., Response criteria for phase II studies of supratentorial malignant glioma, J. Clin. Oncol. 8 (7) (1990) 1277–1280.
[28] P. Karschnia, M. Smits, G. Reifenberger, et al., A framework for standardised tissue sampling and processing during resection of diffuse intracranial glioma: joint recommendations from four RANO groups, Lancet Oncol. 24 (11) (2023) e438–e450.
[29] J. Liu, C. Li, Y. Chen, et al., Diagnostic performance of multiparametric MRI in the evaluation of treatment response in glioma patients at 3T, J. Magn. Reson. Imag. 51 (4) (2020) 1154–1161.
[30] J.E. Park, J.Y. Lee, H.S. Kim, et al., Amide proton transfer imaging seems to provide higher diagnostic performance in post-treatment high-grade gliomas than methionine positron emission tomography, Eur. Radiol. 28 (8) (2018) 3285–3295.
[31] J.E. Park, H.S. Kim, S.Y. Park, et al., Identification of early response to anti-angiogenic therapy in recurrent glioblastoma: amide proton transfer-weighted and perfusion-weighted MRI compared with diffusion-weighted MRI, Radiology 295 (2) (2020) 397–406.
[32] J. Zhang, Y. Wu, Y. Wang, et al., Diffusion-weighted imaging and arterial spin labeling radiomics features may improve differentiation between radiation-induced brain injury and glioma recurrence, Eur. Radiol. 33 (5) (2023) 3332–3342.
[33] Y.S. Chen, S.Y. Zheng, L.L. Huang, et al., Differential diagnostic value of 3.0T MR 3D-ASL technique for recurrence and pseudo-progression of high-grade glioma, Eur. Rev. Med. Pharmacol. Sci. 28 (2) (2024) 679–686.
[34] Y.W. Park, S.S. Ahn, E.H. Kim, et al., Differentiation of recurrent diffuse glioma from treatment-induced change using amide proton transfer imaging: incremental value to diffusion and perfusion parameters, Neuroradiology 63 (3) (2021) 363–372.
[35] S. Jiang, C.G. Eberhart, M. Lim, et al., Identifying recurrent malignant glioma after treatment using amide proton transfer-weighted MR imaging: a validation study with image-guided stereotactic biopsy, Clin. Cancer Res. 25 (2) (2019) 552–561.
[36] W. Zhao, M.E. Robbins, Inflammation and chronic oxidative stress in radiation-induced late normal tissue injury: therapeutic implications, Curr. Med. Chem. 16 (2) (2009) 130–143.
[37] K. Kishi, S. Petersen, C. Petersen, et al., Preferential enhancement of tumor radioresponse by a cyclooxygenase-2 inhibitor, Cancer Res. 60 (5) (2000) 1326–1331.
[38] A. Gao, H. Zhang, X. Yan, et al., Whole-tumor histogram analysis of multiple diffusion metrics for glioma genotyping, Radiology 302 (3) (2022) 652–661.

[39] J. Cheng, J. Liu, H. Yue, et al., Prediction of glioma grade using intratumoral and peritumoral radiomic features from multiparametric MRI images, IEEE ACM Trans. Comput. Biol. Bioinf 19 (2) (2022) 1084–1095.
[40] H. Yu, H. Lou, T. Zou, et al., Applying protein-based amide proton transfer MR imaging to distinguish solitary brain metastases from glioblastoma, Eur. Radiol. 27 (11) (2017) 4516–4524.
[41] J.E. Villanueva-Meyer, R.F. Barajas Jr., M.C. Mabray, et al., Differentiation of brain tumor-related edema based on 3D T1rho imaging, Eur. J. Radiol. 91 (2017) 88–92.
[42] F. Winkler, Y. Kienast, M. Fuhrmann, et al., Imaging glioma cell invasion in vivo reveals mechanisms of dissemination and peritumoral angiogenesis, Glia 57 (12) (2009) 1306–1315.